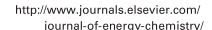


Contents lists available at ScienceDirect

Journal of Energy Chemistry



journal homepage: www.elsevier.com/locate/jechem

Atomic/nano-scale in-situ probing the shuttling effect of redox mediator in Na-O₂ batteries

Kai Yang ^a, Yiwei Li ^a, Langlang Jia ^a, Yan Wang ^a, Zijian Wang ^a, YuChen Ji ^a, Shichun Yang ^b, Magda Titirici ^c, Xinhua Liu ^{b,*}, Luyi Yang ^{a,*}, Feng Pan ^{a,*}

- ^a School of Advanced Materials, Peking University Shenzhen Graduate School, Shenzhen 518055, Guangdong, China
- ^b School of Transportation Science and Engineering, Beihang University, Beijing 100191, China
- ^c Department of Chemical Engineering, Imperial College London, London SW7 2AZ, UK

ARTICLE INFO

Article history: Received 16 July 2020 Revised 11 August 2020 Accepted 11 August 2020 Available online 27 August 2020

Keywords: Na-O₂ battery In-situ AFM EQCM Redox mediator Shuttling effect

ABSTRACT

Sodium-oxygen batteries (Na- O_2) have attracted extensive attention as promising energy storage systems due to their high energy density and low cost. Redox mediators are often employed to improve Na- O_2 battery performance, however, their effect on the formation mechanism of the oxygen reduction product (NaO₂) is still unclear. Here, we have investigated the formation mechanism of NaO₂ during the discharge process in the presence of a redox mediator with the help of atomic/nano-scale *in-situ* characterization tools used in concert (e.g. atomic force microscope, electrochemical quartz crystal microbalance (EQCM) and laser nano-particle analyzer). As a result, real-time observations on different time scales show that by shuttling electrons to the electrolyte, the redox mediator enables formation of NaO₂ in the solution-phase instead of within a finite region near the electrode surface. These findings provide new fundamental insights on the understanding of Na- O_2 batteries and new consequently perspectives on designing high performance metal- O_2 batteries and other related functions.

© 2020 Science Press and Dalian Institute of Chemical Physics, Chinese Academy of Sciences. Published by ELSEVIER B.V. and Science Press. All rights reserved.

1. Introduction

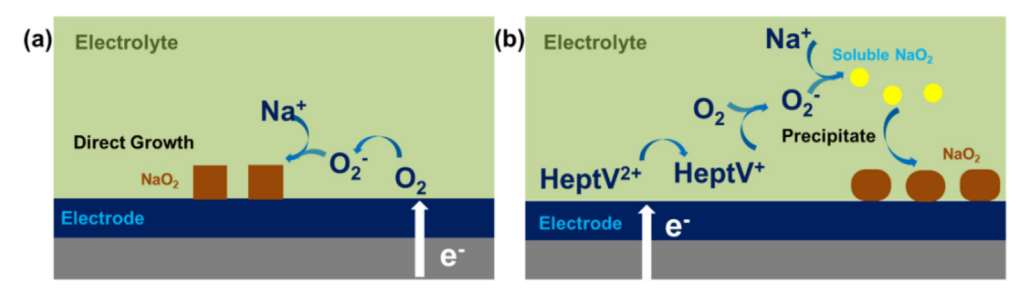
Rechargeable sodium-oxygen (Na-O2) batteries are considered a promising candidate for energy storage devices benefiting from their high theroretical capacity (1100 Wh kg⁻¹), low cost, small charging overpotential, and improved coulombic efficiency compared with lithium-oxygen batteries (Li-O₂) [1-4]. However, Na-O₂ batteries are even further from comercialization comapred with Li-O₂ because of several critical chanllenges: limited rate performance, undesirable side reactions and poor cyclibility [5]. Among many efforts made to improve the performances of metal-O₂ batteries, one promising strategy is employing homogeneous catalysts which are also known as redox mediators [1.6.7]. Unlike lithiumoxygen batteries. Na-O₂ batteries are exempted from high charge overpotentials. Therefore, studies involving redox mediators mainly focus on improving the kinetics of oxygen reduction reactions (ORRs) [8-10]. During ORRs, the redox mediators will work as an intermediate charge carriers between the electrode and the active species (i.e. O2) so that lower energetic barriers and faster

E-mail addresses: liuxinhua19@buaa.edu.cn (X. Liu), yangly@pkusz.edu.cn (L. Yang), panfeng@pkusz.edu.cn (F. Pan).

reaction kinetics can be achieved (Scheme 1a) [6,8,11,12]. There is a debate in the literature on the operating mechanisms of redox mediators, whether the discharging products are directly formed on the electrode surface or in the electrolyte solution instead of within a finite region near the electrode surface. Many reliable analytical results revealing the reaction mechanism of Na-O₂ batteries have been reported [13–16], however, direct and *in-situ* observation of the whole process still remains challenging.

In this work, different *in-situ* characterization techniques (such as *in-situ* atomic force microscope (AFM), EQCM, etc.) have been combined to investigate the shuttling effect of the redox mediator (HeptVBr₂) assisted discharging process in Na-O₂ batteries (Scheme 1b). The formation and decomposition process of NaO₂ has been monitored by *in-situ* characterizations from atomic to nano level. It is revealed that instead of being directly reduced on the electrode, the redox mediator works as a shuttling agent to transfer electrons from electrode surface to the electrolyte solution, and enables formation of NaO₂ in the solution-phase and allows the reaction to take place far from the electrode surface instead of within a finite region near the electrode surface, further resulting in an improved discharging capacity and optimized utilization of the solvated O₂ in the electrolyte.

^{*} Corresponding authors.



Surface dominant

Shuttling effect

Scheme 1. Model shows the shuttling effect of the HeptVBr2 on the formation of NaO2.

2. Experimental

2.1. Preparation of electrolyte and electrode

Diethylene glycol dimethyl ether (DEGDME) is purchased from Acros. Sodium bis (trifluoromethane sulfommide) (NaTFSI) is purchased from Sigma-Aldrich. HeptVBr $_2$ is synthesized according to the previous literature [17]. The electrolyte is prepared by dissolving 0.5 M L $^{-1}$ NaTFSI and 0.5 M L $^{-1}$ HeptVBr $_2$ in DEGDME. The cathode is prepared by mixing acetylene black (ABC) and polyvinylidene difluoride (PVDF) in n-methyl pyrrolidone (NMP, Aladdin) with the weight ratio of 2:1. Then the mixture slurry is casted on carbon paper (diameter = 15 mm). The real loading of the active material is 0.7 mg cm $^{-2}$, followed by drying at 80 °C for 24 h under vacuum.

2.2. Electrochemical measurements

The cells are assembled in an Ar-filled glove box. Sodium foil is used as the counter electrode and a glass fiber is used as separator. 120 μ L of electrolyte (0.5 M L $^{-1}$ NaTFSI in DEGDME, with/without 5 mM L $^{-1}$ HeptVBr $_2$) is added during cell assembling. The CV is measured using a CHI660E electrochemical workstation based on a three-electrode system. The galvanostatic charge and discharge tests are conducted using a Neware battery testing system in an O $_2$ saturated box.

2.3. In-situ AFM test

An in-situ cell is assembled as shown in Fig. S1. The highly oriented pyrolytic graphite (HOPG, 12 mm × 12 mm, ZYB Grade, Bruker Corporation) is used as working electrode. The HOPG is cleaved with adhesive tapes before in situ tests. The sodium metal ring is used as reference and counter electrode. A solution of 0.1 mL electrolyte is injected into the *in-situ* cell in every test. The electrolyte is saturated with O2 before using. The whole in situ cell is connected to a CHI660C electrochemical workstation (Chenhua Instument Co., Ltd., China) for cyclic voltammetry (CV) tests. In-situ imaging of the reaction is accomplished with Bruker Multimode 8 system in an Argon glovebox (MIKOUNA, H₂O < 0.1 ppm, $O_2 < 0.1$ ppm). All the images are taken in Scansyst-fluid mode with an insulating silicon nitride AFM tip. The images are captured at a rate of 0.5 Hz. *In-situ* AFM images are taken at different potentials. During discharging process, the potential is swept from OCP to 1.0 V (vs. Na/Na⁺) followed by a positive sweeping back to 4.0 V (vs. Na/Na⁺).

2.4. EQCM weighing of the discharging product

EQCM measurements are performed using a QCM922 quartz crystal microbalance in conjunction with a VersaSTAT 3 Poten-

tiostat/Galvanostat. The goad-coated quartz crystals are used as the working electrodes (reference frequency of 9 MHz), a platinum electrode and an Ag/AgCl electrode are used as counter and reference electrode respectively. The EQCM experiments are performed at a scan rate of 1 mV s $^{-1}$ in the voltage range 1.0 V to 4.0 V (vs. Na/Na $^{+}$). A solution of 3 mL electrolyte (with/without HeptVBr $_{2}$) saturated with O $_{2}$ is added to the EQCM cell during each experiment. The mass change during the electrochemical reaction is calculated as the following equation:

$$\Delta f = -\frac{2f_0^2}{A\sqrt{\rho_Q\mu_Q}}\Delta m$$

where Δf is the frequency change of the gold-coated quartz crystal electrode, f_0^2 is the resonant frequency of the quartz crystal, A is the active crystal surface, $\rho_{\rm Q}$ is the density of quartz (2.648 g cm $^{-3}$) and $\mu_{\rm Q}$ is the shear modulus of quartz (2.947 \times 10 11 g cm $^{-1}$ s $^{-2}$).

The average molecular weight (M_w) during the electrochemical reaction is calculated by:

$$M_{\rm w} = -\frac{\Delta mF}{\Delta Q}$$

where Δm is the mass change of the selected electrochemical process, ΔQ is the electron participated in the reaction, and F is the Faraday's constant (~96485 C mol⁻¹)

2.5. In-situ laser nano-particle size measurement

The setup of *in-situ* particle size measurement is shown as Fig. 5 (a). A laser particle analyzer (Zetasizer Nano Particle Size Analysis) and a CHI1030C electrochemical workstation are cooperated to monitor the *in-situ* particle size evolution in the electrolyte solution. To make a robust and conductive cathode, the cathode slurry (ABC mixed with PVDF in NMP with the weight ratio of 2:1) is casted on nickel mesh followed by vacuum drying at 80 °C overnight. The sodium wire is used as counter and reference electrode. The particle size is measured and recorded at different potentials. The potential range is 1.0 V to 4.0 V (vs. Na/Na $^+$).

2.6. Material characterization

The discharged HOPG and the gold-coated quartz crystal electrodes were removed from the cell and washed by CH₃CN to remove residual electrolyte and dried in an Argon glovebox before characterization. The phases are analyzed using X-ray diffraction (XRD, Bruker D8 Advance diffractometer using Cu K_{α} radiation, λ = 1.5405 Å).

3. Results and discussion

3.1. Electrochemical performances

In our previous work [17], HeptVBr₂ (molecular structure is shown in Fig. 1) has been developed as an effective additive to enhance the discharging/charging performance in Li-O₂ batteries: HeptV⁺ facilitated the formation of toroid-shaped Li₂O₂ in the solution and promoted the ORR process to increase the discharging process. Inspired by this, herein, 5 mM L⁻¹ HeptVBr₂ was added to the diethylene glycol dimethyl ether (DEGDME) based electrolyte to test whether it could enhance the Na-O₂ battery performances. As shown in Fig. 1, the introduction of HeptVBr₂ could

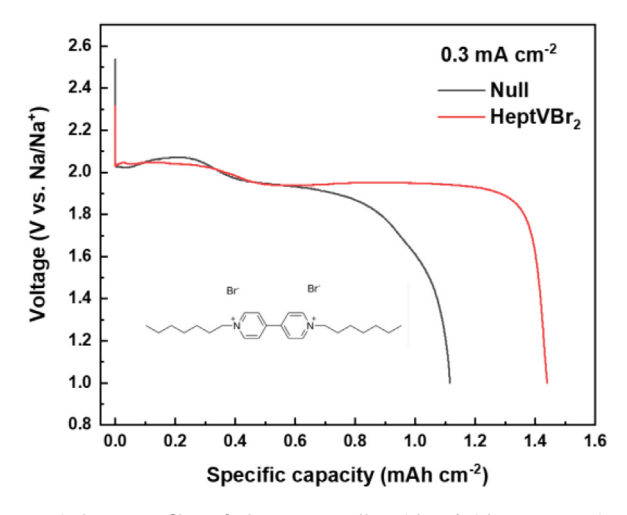


Fig. 1. Discharge profiles of the Na-O $_2$ cells without/with HeptVBr $_2$ in the electrolyte of 0.5 M L $^{-1}$ NaTFSI in DEGDME. The current density is 0.3 mA cm $^{-2}$ and voltage cuts off at 1.0 V (vs. Na/Na $^{+}$).

improve the discharge capacity effectively. However, the mechanism of this effect is still controversial whether the redox mediator-assisted reaction is surface-dominant. The reaction of the redox mediator and the solvated O_2 in the electrolyte solution is unclear either. In this work, efforts have been made to unravel the puzzle through the cooperation of different *in-situ* characterizations.

3.2. In-situ AFM observation of NaO2 formation

In recent years, in-situ AFM has been developed and widely accepted as a powerful tool to visualize the evolution of the electrode surfaces in lithium batteries [18-20]. In this work, in-situ AFM was utilized as a visualization tool to observe real-time NaO₂ growth process. Fig. S1 shows the setup of the in-situ AFM cell. Highly oriented pyrolytic graphite (HOPG) was employed as the working electrode, and a sodium ring served as the counter and reference electrodes. The electrolyte was saturated with O₂ before testing. Fig. 2 presents the AFM scanning result in the electrolyte without additive. The cyclic voltammetry (CV) curve of the in-situ AFM is shown in Fig. S2. Higher peak currents can be observed in the presence of HeptVBr₂, which is in good accordance with the improved capacity presented in Fig. 1. As shown in Fig. 2 (a), the HOPG surface was clean at open circuit potential (OCP). During the anodic scanning, the formation of nano-sized particles on the HOPG surface can be observed (shown in Fig. 2b). The particles continuously grew under the anodic current (Fig. 2c and d). When the voltage was scanned back to 3.9 V (vs. Na/Na⁺) (Fig. 2e and f), some of the particles disappeared while some part of the HOPG surface was still covered with nano-particles. This indicates that the discharging product couldn't be totally oxidized, and the coulombic efficiency was not high enough. Fig. S3 presents the morphology of the discharging product, i.e. the cubic nano particles were previously reported to be NaO₂ [13] with the average size of approximately 200 nm.

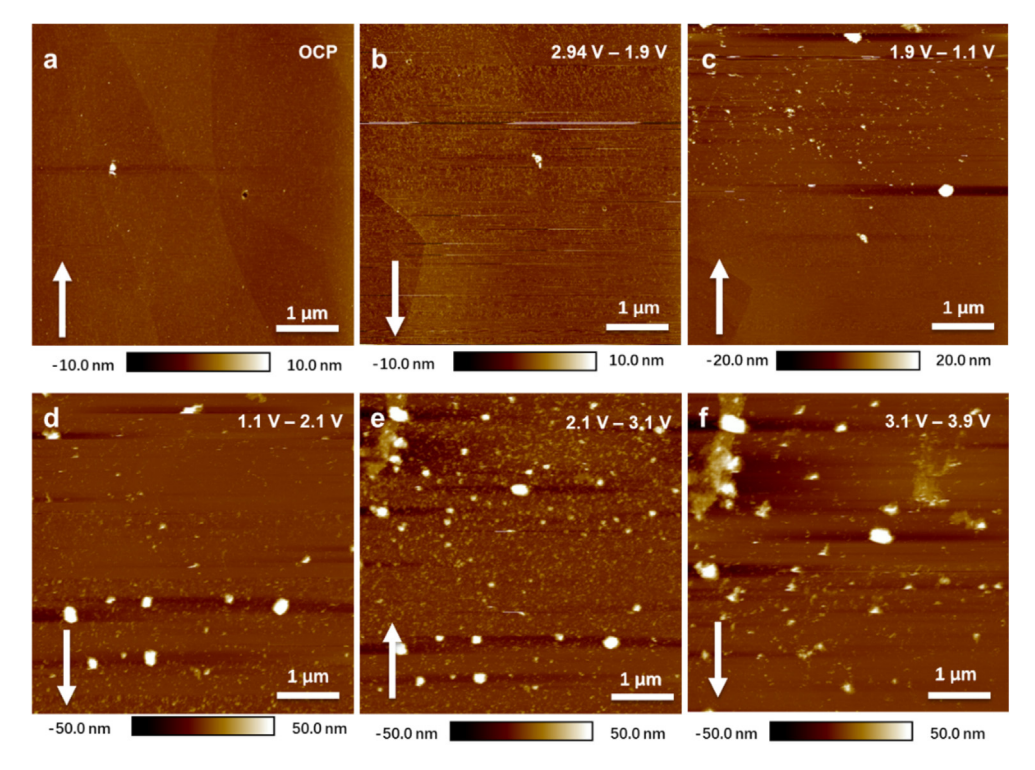


Fig. 2. In-situ AFM scanning without additive. In-situ AFM images taken at (a) OCP, (b) 2.94 V to 1.9 V, (c) 1.9 V to 1.1 V, (d) 1.1 V to 2.1 V, (e) 2.1 V to 3.1 V and (f) 3.1 V to 3.9 V. The white arrows in the images show the scan direction. The CV scan rate is 2 mV s⁻¹ (vs. Na/Na*).

Fig. 3 shows the interfacial evolution processes of HOPG in the presence of HeptVBr₂. During the discharging process, nanoparticles are found to grow on the HOPG surface (Fig. 3b). There were some differences with the addition of HeptVBr₂ when lower scanning voltages were applied. Figs. S4 and S5 demonstrate the optical images captured applying different scanning voltages during the *in-situ* AFM scanning. It should be noted that the electrolyte was clear during the whole AFM scanning when there was no additive. After the addition of HeptVBr₂, the electrolyte became cloudy at low voltage, lowering the reflection density of AFM laser (The AFM detector collected the reflection of laser from probe to image was shown in Fig. S6a). As a result, the sum value of AFM laser became too low to be collected when the voltage was scanned from 2.0 V to 1.0 V (vs. Na/Na⁺). When the voltage was scanned back

anodically, the electrolyte gradually became clear so that the AFM scanning could be carried on. As shown in Fig. 3(c), the HOPG surface was covered with discharging product at 2.0 V (vs. Na/Na⁺). When charged back to 4.0 V (vs. Na/Na⁺) (Fig. 3d and e), most of the discharging product would decompose from the HOPG surface, further proving the improvement of the coulombic efficiency. The CV profile in Fig. S2 shows that the higher peak current was obtained with HeptVBr₂ which is consistent with the AFM observation.

Using AFM, the morphology of discharging products in different electrolytes is also compared in Fig. 4. After the addition of HeptVBr₂, the HOPG surface was covered with more ellipsoidal discharging product with uniform particle sizes during discharging (details were shown in Fig. S7); whereas the discharging product became cubic and sparse without additive. The AFM probes were

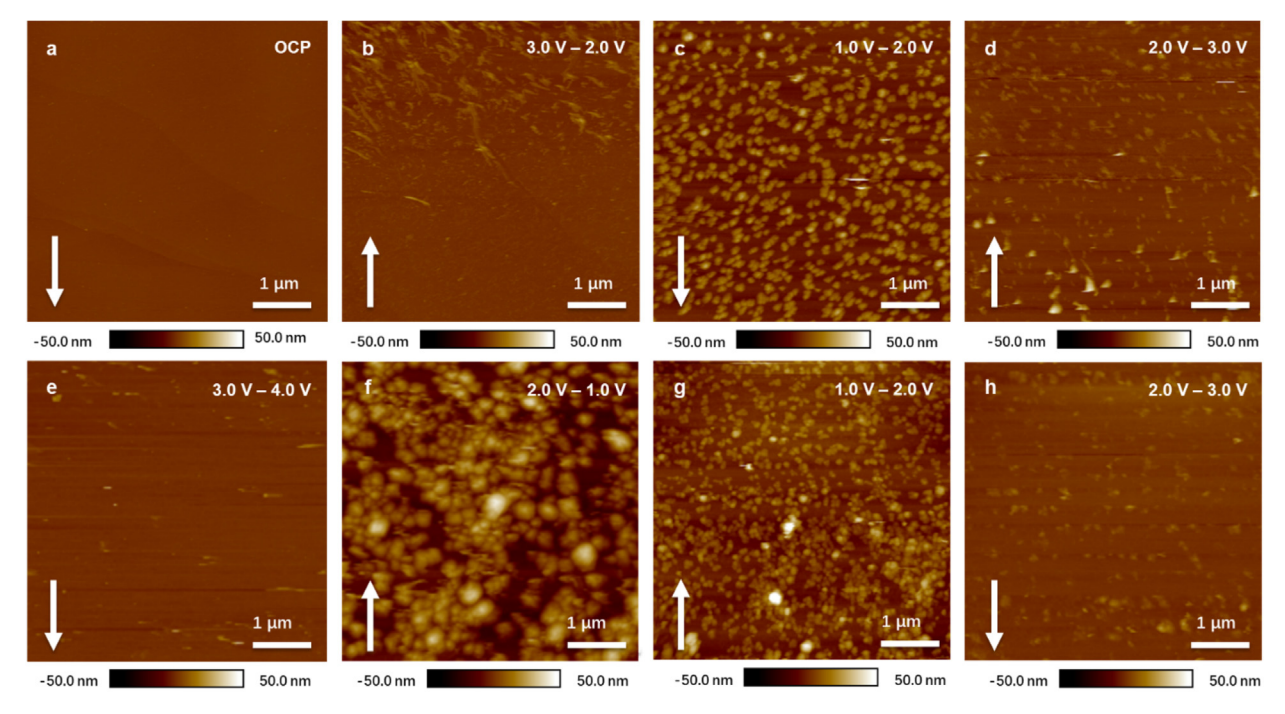


Fig. 3. In-situ AFM scan with 5 mM L^{-1} HeptVBr₂ additive. In-situ AFM images taken at (a) OCP, (b) 3.0 V to 2.0 V, (c) 1.0 V to 2.0 V, (d) 2.0 V to 3.0 V and (e) 3.0 V to 4.0 V during first cycle. During the second cycle: (f) 2.0 V to 1.0 V, (g) 1.0 V to 2.0 V and (h) 2.0 V to 3.0 V. The white arrows in the images show the scan direction. The CV scan rate is 2 mV s⁻¹ and the voltage range is 1.0 V to 4.0 V (vs. Na/Na*).

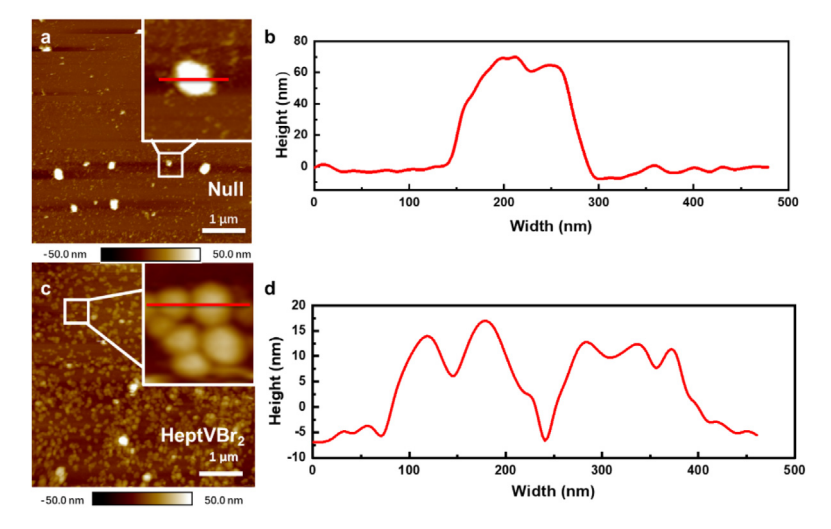


Fig. 4. AFM images show the different morphologies on HOPG. Without additive: (a) AFM images taken in the discharge process and (b) height profile of the enlarged figure (a). With 5 mM L⁻¹ HeptVBr₂: (c) AFM images taken in the discharging process and (d) height profile of the enlarged figure (c).

taken out for optical observation. During the AFM scanning (Fig. S6a), the back of the cantilever should be clean because it is far away from the sample. The cantilever of the probe kept clean when scanned in the electrolyte without additive (before scanning: Fig. S6b and after scanning: Fig. S6d), while the cantilever was covered with residues when used in the electrolyte with HeptVBr₂ (before scanning: Fig. S6c and after scanning: Fig. S6e). Therefore, the AFM results shown above suggest that the discharging product might form in the solution with the addition of HeptVBr₂.

3.3. Weighing the NaO₂ formation by EQCM

Electrochemical Quartz Crystal Microbalance (EQCM) allows researchers to precisely weigh the mass change of the reaction product during the electrochemical process [19]. EQCM was employed in our work to observe the NaO₂ formation without/with HeptVBr₂.

The mass change (Δm) and the average molecular weight (M_w) during the electrochemical reaction is calculated as the following equation (detailed definitions of the parameters are described in the Experiment Section):

$$\Delta f = -\frac{2f_0^2}{A\sqrt{\rho_{\rm Q}\mu_{\rm Q}}}\Delta m \tag{1}$$

$$Mw = -\frac{\Delta mF}{Q} \tag{2}$$

The cathodic peak was selected to calculate the mass change with electron transferred. As shown in Fig. 5(a), the mass change in the DEGDME-based electrolyte without additive was calculated to be 56.4 g mol⁻¹ approximately, which is very close to the molecular weight of NaO₂ (55 g mol⁻¹), indicating almost all electrons released from the working electrode was reacted on the electrode surface, and the discharging product (NaO₂) is electrochemically reduced from O2 (Eq. (3)) [21].

$$O_2 + Na^+ + e^- \rightarrow NaO_2 \tag{3}$$

After the EQCM tests, the electrode was taken out for XRD analysis. The electrode was washed with CH_3CN to remove the residue electrolyte. The XRD result in Fig. S8 shows the typical XRD pattern of NaO_2 [22–24]. As shown in Fig. 5(b), in the presence of HeptVBr₂, the calculated value was 29.4 g mol⁻¹ which was much smaller than the theoretical value, indicating a different reaction path and mechanism. Here, it can be demonstrated that the introduction of redox mediator could change the reaction pathway in which $HeptV^{2+}$ would firstly electrochemically capture the electron, forming $HeptV^{+}$ radical, and then followed by two chemical reactions (Eqs. (4) and (5)) [8,17]:

$$HeptV^{2+} + e^- \rightarrow HeptV^+ \eqno(4)$$

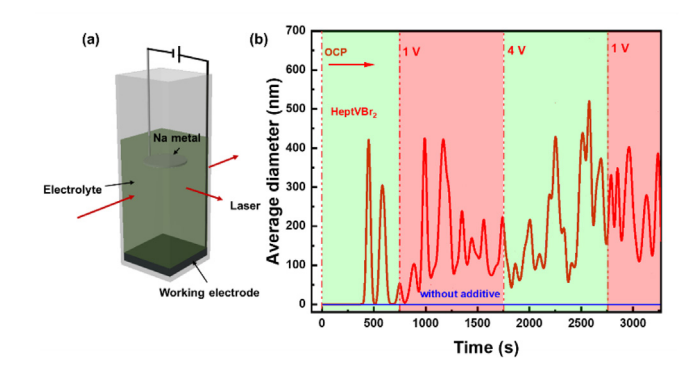


Fig. 6. *In-situ* laser particle size measurement. (a) Schematic of the setup of the particle size measurement. (b) The particle size evolution in the solution during the discharge–charge process. The scan rate is 2 mV s^{-1} (vs. Na/Na $^+$). Blue and red lines present the particle size evolution without additive and with HeptVBr $_2$, respectively.

$$HeptV^{+} + O_2 \rightarrow HeptV^{2+} + O_2^{-}$$
 (5)

Consequently, the combination between Na-ion and superoxide radical could occur in the solution and the formed NaO $_2$ will gradually precipitate on the electrode, hence the slower mass change. However, it should be noted that different from the NaO $_2$ formed through direct electrochemical reduction, the precipitated NaO $_2$ could be easily washed away by CH $_3$ CN, so there was no obvious NaO $_2$ XRD pattern in Fig. S8.

3.4. In-situ particle size measurement

To further confirm the solution-phase reaction mechanism during discharging, a self-made in-situ laser nano-particle size measurement (the setup is shown in Fig. 6a) was conducted to observe the particle formation in the electrolyte during discharging. When the pure electrolyte was used, the measured average diameter was zero throughout the test which confirmed that no solid product formed in the electrolyte (blue line in Fig. 6b). After the addition of HeptVBr₂, a different phenomenon was observed. As shown in Fig. 6(b), no particles were detected at the early stages of the discharging process (red line). When reduced to about 2.0 V (vs. Na/Na⁺), nanoparticles appeared in the solution with an average particle size of 300 nm (CV curve was shown in Fig. S9). During the oxidation process, the average particle size shrunk to 150 nm, which could be due to the fact that the discharging product with larger sizes precipitated onto the electrode. Further, during the discharging process, similar results can be observed, suggesting this process is reversible. The result of the in-situ particle size measurement further confirmed the solution-phase formation of discharging product after the addition of redox mediator.

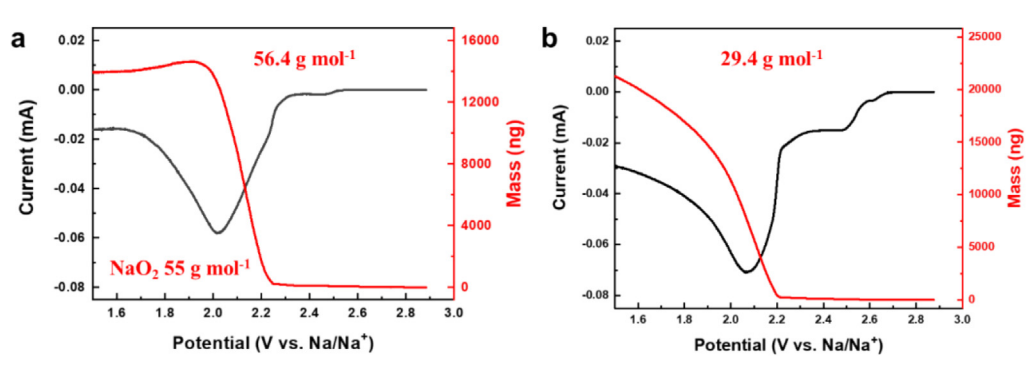


Fig. 5. EQCM tests show the CV and mass changes of the discharging process. (a) Without additive and (b) with 5 mM L⁻¹ HeptVBr₂. The scan rate is 2 mV s⁻¹ (vs. Na/Na*).

4. Conclusions

In summary, we successfully combined several atomic/nano insitu characterization to monitor the real-time formation of NaO₂ in DEGDME-based electrolyte from multi-scale perspective. First, insitu AFM was employed to record the morphology change of the HOPG surface and the discharging product formation. The additive of HeptVBr2 changes the morphology of NaO2 from cubic to ellipsoidal. Further, EQCM was employed to monitor the accurate mass change during discharging. When no additive was used, the mass change was calculated to be 56.4 g mol⁻¹ which was close to the theoretical value of NaO₂ (55 g mol⁻¹) indicating a surfacedominant reaction mechanism. While the mass change was much smaller after the addition of HeptVBr₂ (29.4 g mol⁻¹), the NaO₂ was demonstrated to form in the electrolyte solution instead of within a finite region near the electrode surface. In addition, the in-situ laser nano-particle size measurement was carried out to observe the particle size evolution in the electrolyte. No solid product was observed in the absence of HeptVBr2, while particle size evolution was observed in electrolyte with HeptVBr₂. By the cooperation of atomic/nano-scale in-situ characterization tools, a solutionphase reaction mechanism of NaO₂ growth and the shutting effect of the redox mediator were demonstrated and confirmed (as shown in Scheme 1). Without the addition of HeptVBr₂ (Scheme 1a), the electron released from the electrode was captured and reacted by O₂ dissolved in the electrolyte. The formed O₂ could then react with the sodium ion to form the NaO2 on the electrode surface. The whole reaction is surface-dominant. With HeptVBr₂ (Scheme 1b), the electron released from the electrode was firstly captured by HeptV²⁺ to form HeptV⁺, and then reduce the O₂ dissolved in the electrolyte to form O_2^- . Finally, the sodium ions could react with O_2^- to form soluble NaO₂ and then precipitate to the electrode surface. The HeptVBr2 works as a shuttling agent to transfer electrons from electrode surface to the O2 solvated in the electrolyte solution, so the NaO2 could form even in the solution far away from the electrode surface. The proposed method demonstrates a general approach to investigate the mechanism in Na-O2 batteries and other energy storage devices, providing visual evidence and effective characterization approach to investigate charging/discharging reaction mechanisms.

Declaration of Competing Interest

The authors declare that they have no known competing financial interests or personal relationships that could have appeared to influence the work reported in this paper.

Acknowledgments

This research was financially supported by Soft Science Research Project of Guangdong Province (No. 2017B030301013), the Shenzhen Science and Technology Research (Grant No. JCYJ20170818085823773, ZDSYS201707281026184), China Postdoctoral Science Foundation (2019M660317) and the National Science Foundation of China (No. U1864213).

Appendix A. Supplementary data

Supplementary data to this article can be found online at https://doi.org/10.1016/j.jechem.2020.08.025.

References

- [1] X. Bi, R. Wang, K. Amine, J. Lu, Small Methods 3 (2019) 1800247.
- [2] J. Xiang, L. Yang, L. Yuan, K. Yuan, Y. Zhang, Y. Huang, J. Lin, F. Pan, Y. Huang, Joule 3 (2019) 2334–2363.
- [3] C.-S. Yang, K.-N. Gao, X.-P. Zhang, Z. Sun, T. Zhang, Rare Metals 37 (2018) 459-
- [4] Y. Ren, S. Zhao, H. Li, S. Zhang, J. Liu, Y. Xiao, J. Energy Chem. 30 (2019) 63-70.
- [5] Y. Zhu, F. Yang, M. Guo, L. Chen, M. Gu, ACS Nano 13 (2019) 14399-14407.
- [6] I. Landa-Medrano, I. Lozano, N. Ortiz-Vitoriano, I. Ruiz de Larramendi, T. Rojo, J. Mater. Chem. A 7 (2019) 8746–8764.
- [7] L. Yang, J.T. Frith, N. Garcia-Araez, J.R. Owen, Chem. Commun. 51 (2015) 1705– 1708
- [8] J.T. Frith, I. Landa-Medrano, I. Ruiz de Larramendi, T. Rojo, J.R. Owen, N. Garcia-Araez. Chem. Commun. 53 (2017) 12008–12011.
- [9] D. Schröder, C.L. Bender, R. Pinedo, W. Bartuli, M.G. Schwab, Ž. Tomović, J. Janek, Energy Technol. 5 (2017) 1242–1249.
- [10] W.-W. Yin, Z.-W. Fu, Chem. Commun. 53 (2017) 1522–1525.
- [11] J.-B. Park, S.H. Lee, H.-G. Jung, D. Aurbach, Y.-K. Sun, Adv. Mater. 30 (2018) 1704162.
- [12] X. Shen, S. Zhang, Y. Wu, Y. Chen, ChemSusChem 12 (2019) 104-114.
- [13] I.M. Aldous, L.J. Hardwick, Chem. Commun. 54 (2018) 3444-3447.
- [14] W.-J. Kwak, L. Luo, H.-G. Jung, C. Wang, Y.-K. Sun, ACS Energy Lett. 3 (2018) 393–399
- [15] Z. Liang, Q. Zou, Y. Wang, Y.-C. Lu, Small Methods 1 (2017) 1700150.
- [16] L. Lutz, W. Dachraoui, A. Demortière, L.R. Johnson, P.G. Bruce, A. Grimaud, J.-M. Tarascon. Nano Lett. 18 (2018) 1280–1289.
- [17] H. Liu, M. Liu, L. Yang, Y. Song, X. Wang, K. Yang, F. Pan, Chem. Commun. 55 (2019) 6567–6570.
- [18] L. Lin, K. Yang, R. Tan, M. Li, S. Fu, T. Liu, H. Chen, F. Pan, J. Mater. Chem. A 5 (2017) 19364–19370.
 [19] T. Liu, L. Lin, X. Bi, L. Tian, K. Yang, J. Liu, M. Li, Z. Chen, J. Lu, K. Amine, K. Xu, F.
- Pan, Nat. Nanotech. 14 (2019) 50–56.
- [20] K. Yang, L. Jia, X. Liu, Z. Wang, Y. Wang, Y. Li, H. Chen, B. Wu, L. Yang, F. Pan, Nano Res. 13 (2020) 412–418.
- [21] K.-X. Wang, Q.-C. Zhu, J.-S. Chen, Small 14 (2018) 1800078.
- [22] X. Bi, R. Wang, L. Ma, D. Zhang, K. Amine, J. Lu, Small Methods 1 (2017) 1700102.
- [23] G.A. Elia, I. Hasa, J. Hassoun. Electrochim. Acta 191 (2016) 516-520.
- [24] P. Hartmann, C.L. Bender, J. Sann, A.K. Dürr, M. Jansen, J. Janek, P. Adelhelm, PCCP 15 (2013) 11661–11672.